

Robust Task Scheduling for Heterogeneous Robot Teams under Capability Uncertainty

Bo Fu, William Smith, Denise Rizzo, Matthew Castanier, Maani Ghaffari, and Kira Barton

Abstract—This paper develops a stochastic programming framework for multi-agent systems where task decomposition, assignment, and scheduling problems are simultaneously optimized. Due to their inherent flexibility and robustness, multi-agent systems are applied in a growing range of real-world problems that involve heterogeneous tasks and uncertain information. Most previous works assume a unique way to decompose a task into roles that can later be assigned to the agents. This assumption is not valid for a complex task where the roles can vary and multiple decomposition structures exist. Meanwhile, it is unclear how uncertainties in task requirements and agent capabilities can be systematically quantified and optimized under a multi-agent system setting. A representation for complex tasks is proposed to avoid the non-convex task decomposition enumeration: agent capabilities are represented as a vector of random distributions, and task requirements are verified by a generalizable binary function. The conditional value at risk (CVaR) is chosen as a metric in the objective function to generate robust plans. An efficient algorithm is described to solve the model, and the whole framework is evaluated in two different practical test cases: capture-the-flag and robotic service coordination during a pandemic (e.g., COVID-19). Results demonstrate that the framework is scalable, generalizable, and provides low-cost plans that ensure a high probability of success.

Index Terms—Heterogeneous multi-agent systems, Task allocation, Stochastic vehicle routing problem, Scheduling and coordination, Pandemic robotic services

I. INTRODUCTION

TECHNOLOGICAL advances in sensing and control have enabled robotic applications in an ever-growing scope. On the other hand, the growing complexity and requirements of the applications soon exhaust the capability of a single robot: limited by design rules and actuator/sensor power, even the most competent robot is not able to handle all real-world tasks alone. This trend fosters the recent proliferation of multi-agent system applications in agriculture [1], warehouse management [2], construction [3], defense [4], exploration [5]–[9], and surveillance [10]–[12]. The advantages of replacing a large omnipotent robot with a team of smaller and less powerful robots include the robustness to agent failures, resilience of team configuration, and lower maintenance costs (a large robot

Manuscript received: Month, Day, Year; Revised Month, Day, Year; Accepted Month, Day, Year.

DISTRIBUTION A. Approved for public release; distribution unlimited. (OPSEC 5240)

Bo Fu, Maani Ghaffari, and Kira Barton are with the University of Michigan, Ann Arbor, MI 48109, USA (e-mail: bofu@umich.edu; maanig@umich.edu; bartonkl@umich.edu)

William Smith, Denise Rizzo, and Matthew Castanier are with the US Army DEVCOM Ground Vehicle Systems Center, Warren, MI 48397, USA (e-mail: william.c.smith1019.civ@mail.mil; denise.m.rizzo2.civ@mail.mil; matthew.p.castanier.civ@mail.mil)

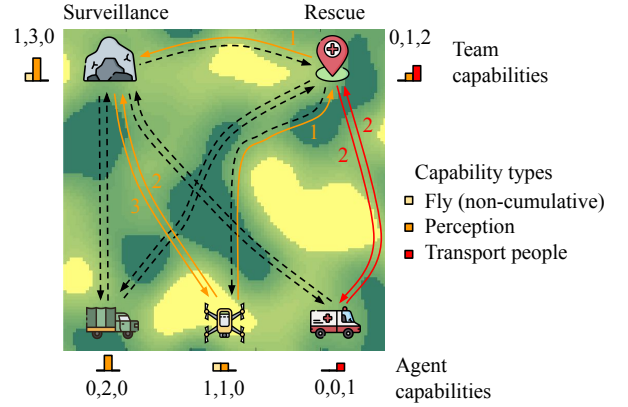


Fig. 1: Graphical model: an example of the heterogeneous teaming problem (HTP) with two tasks and three agent species. A graphical model links agents and tasks. There are three types of capabilities: fly, perception, and transport people. The rescue task requires the ability to transport people, but also perception to guide the process. While the surveillance task requires both flying and perception capabilities as the task is performed in a small mountain. We regard the capability to fly as non-cumulative (the team can fly only when all agents in the team can fly).

with the same task capabilities is usually harder to design and costlier due to the system complexity) [13].

The reason that a team of less powerful robots can achieve the same or more complex tasks with the above advantages is that the functional heterogeneity within the team, i.e., distinct sensor and actuator capabilities of the robots, can complement each other during a task. In contrast to structural heterogeneity (e.g., maximum velocity or energy capacity), functional heterogeneity usually leads to fundamental differences between task capabilities (e.g., the ability to fly or remove debris) [14].

The fundamental problems [15] that arise when applying a functionally heterogeneous multi-agent system to a mission containing multiple complex sub-tasks include: understanding how to decompose the tasks into elements that can be assigned to a single agent (how), determining which agents should be assigned to a particular task element (who), and deriving a schedule that enables the heterogeneous team to successfully complete the task (when). I.e., consider the whole problem as a task allocation; then, task allocation = task decomposition + assignment + scheduling.

A task is considered complex if there exist multiple decompositions and it is unknown which decomposition should be selected without simultaneously considering task assignment and schedule planning (e.g. the problem is coupled) [15]. One modeling option is to enumerate all decomposition possibilities, but such an enumeration discretizes the feasible problem space and adds non-convex constraints to the optimization. As a result, the solver may need to enumerate the decomposition

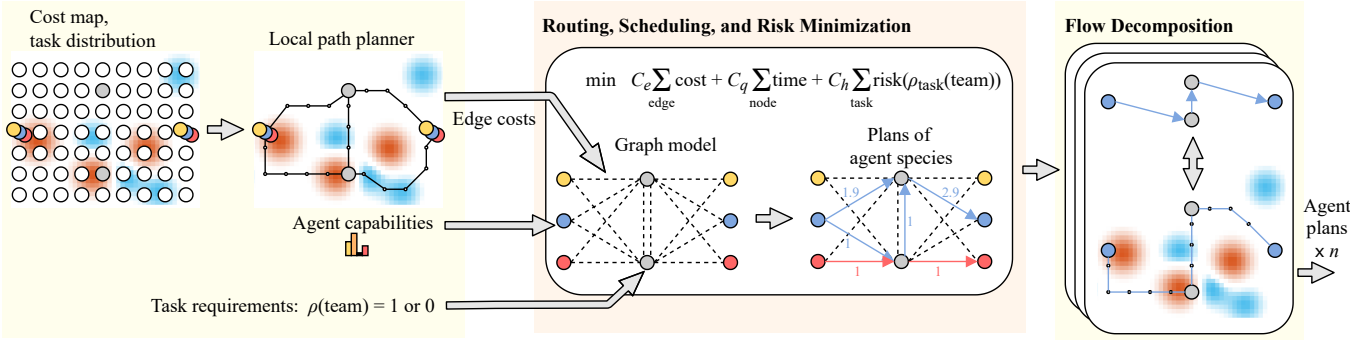


Fig. 2: System architecture. Input: cost (energy) maps, agent capabilities, and task requirements. Output: agent routes, schedules, and team formations. There are two major components. A routing, scheduling, and risk minimization model (Sec. III) generates a network flow for each agent species. And then these networks are further decomposed into individual agent plans through a flow decomposition model (Sec. V).

cases, which could result in an exponentially growing computation cost. Therefore, in the representation of the constraints between complex tasks and heterogeneous agents, high non-convexity and discreteness, such as enumerations of decomposition, should be avoided to facilitate the optimization. Namely, convex task representations/constraints are preferred.

Among the few previous works that deal with functional heterogeneity in a complex task setting, most optimization models are designed for use with a specific application. Therefore, in addition to a convex representation, there is a need for fundamental methods that provide a more systematic representation that can generalize within a larger scope of complex tasks.

An important aspect to consider when dealing with dynamic systems is the concept of uncertainty. To capture the effects of uncertainty within the decision making process, we must consider the design of a robust framework. In this work, we consider uncertainties within the task requirements and agent capabilities.

In this paper, we present a **Capability-based robust Task Assignment and Scheduling (CTAS)** framework to optimize task decomposition, assignment, and scheduling simultaneously within a closer to convex stochastic task model, which can generalize to multiple practical scenarios. Figure 1 shows a graphical model for a small example problem. Consider a set of heterogeneous agents (can be robots/vehicles/humans) and complex tasks; the proposed framework will form agent teams, schedules, and routes to minimize energy and time costs for completing the task combined with the risk of non-completion. We define this class of problems as the heterogeneous teaming problem (HTP). The system architecture is summarized in Fig. 2 and will be discussed in the following sections.

A. Contributions

In [16], we dealt with a deterministic variation of such a problem, where we assumed exact information (instead of a distribution) of the agent capabilities and task requirements was known. In this work, we develop a generalizable framework for task assignment and scheduling that systematically represents heterogeneous and uncertain task requirements and agent capabilities. This paper provides the following contributions.

- 1) The development of a modeling framework that captures uncertainties within the task requirements and agent capabilities.
- 2) The derivation of a cost function that incorporates the concept of risk within the minimization.
- 3) Reformulation of the heterogeneous teaming problem (HTP) to provide a more scalable algorithm that is solved by using a flow decomposition sub problem.
- 4) A comprehensive evaluation approach that provides a demonstration of the relevant contributions as well as a comparison of the task assignment performance to a baseline algorithm.

B. Outline

The remainder of this paper is organized as follows: Sec. II briefly introduces the related work of multi-agent task allocation and concludes with research gaps that this work investigates. Sec. III describes the general problem mathematically and presents a risk minimization framework for the problem. Sec. IV introduces an algorithm to solve the risk minimization problem and output a general routing plan described as network flows of agent movements. Sec. V proposes a network flow decomposition problem to generate routing plans and schedules for individual agents. The two-step process in sections IV and V improves the scalability of the framework compared to a solution method that outputs individual plans directly within one optimization. Sec. VI describes the experiments and results, followed by discussion. Finally, Sec. VII concludes the paper and provides ideas for future work based on current limitations.

II. RELATED WORK

According to the taxonomy in [15], [17], the above-proposed problem is a task allocation problem in the category CD-[ST-MR-TA]: complex task dependencies (CD), single-task robot (ST), multi-robot tasks (MR), and time-extended assignment (TA). It is one of the most challenging task assignment categories and has been considered in few previous works in literature. The time-extended assignment considers scheduling, in contrast to the instantaneous assignment (IA), which only makes matches between tasks and robots.

While there are many previous works about multi-robot tasks, most of them decompose a multi-robot task into elements that can be handled by a single agent in a fixed way. If such a decomposition exists, the task decomposition problem is presolved and decoupled from the assignment and scheduling problem. Many previous works in coalition formation [18], vehicle routing [14], [19], job shop scheduling [20]–[22], and robotic soccer games [23], [24] deal with such non-complex (or compound) tasks. In [19], the tasks are decomposed into roles for medical agents and transport agents while connected with scheduling constraints. In a job shop scheduling problem [21], a job (task) is decomposed into fixed operations that can be executed by a single machine (agent). In [24], a soccer game is also composed of multiple roles that can be later assigned to a specific agent based on utility maximization.

Among the systems that deal with complex tasks, [25], [26] model the constraints between fire extinguishing and debris removal tasks such that at least one ‘clear’ route to a fire extinguishing task can be identified. Since the solution set contains multiple combinations, the whole problem is deemed complex. [11] models the specific recharging behaviors of an unmanned aerial/ground vehicle team under a coverage problem. While these examples demonstrate approaches for dealing with complex tasks, the models used in these examples are specific to the application and do not generalize to other examples.

There are some methods for formulating complex tasks that can generalize and avoid a naive enumeration of role or action combinations. In [27]–[33], a task is represented as a graph of states (nodes) and actions (edges) using planning domain definition language (PDDL) [34] that is domain-independent once the language is defined. Moreover, there are variants of PDDLS for multi-agent problems [35]. [36], [37] use a Bayesian network representation consisting of tasks, observations, constraints, and action nodes. Hierarchical tree networks (HTN) are used in [38]–[41] to represent tasks where leaf nodes are roles for assignment. A tree structure representation utilizes the hierarchical nature of a task and partially avoids enumerations. However, these representations are usually applied to systems with less than five agents. The number of states in such trees/graphs could explode rapidly with respect to the number of agents and decomposition choices. Such a scalability issue limits its application to larger multi-agent systems.

Uncertainty exists widely in the estimation of task requirements and agent capabilities. More recent works capture such uncertainty explicitly in their models. [42] models the agent action uncertainty during single-robot tasks in Markov decision processes (MDP). However, instead of modeling the joint space of multiple tasks as a large MDP through concatenation, they use linear temporal logic to describe the relationship between these task MDPs, limiting the dimensionality of the integrated problem. Each MDP is solved beforehand, and jointly the probability of completing the tasks is maximized. In [23], [24], [43], an agent’s capabilities are represented as a Gaussian random vector where the uncertainty is captured in the distribution. A task requirement is then specified by the

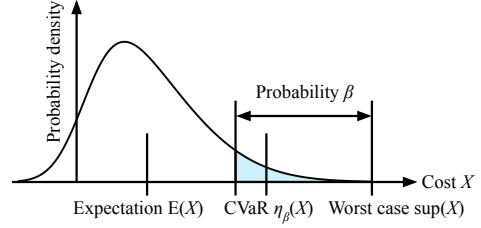


Fig. 3: Graphical illustration of CVaR, defined as expected cost of the worst β -proportion of the cases. Denoted as $\eta_\beta(\cdot)$, it is a function of the random distribution with β as a hyper-parameter.

Table I: A comparison between STRATA and CTAS. The meaning of ‘and/or’ in the task requirements is defined in Sec. III. STRATA claims that it can deal with noncumulative capability types (such as the speed of an agent). However, it thresholds on a value and then treats the binary value after thresholding in the same way as a cumulative capability. For noncumulative types, we require instead that all agents in the team meet the minimum requirement.

	STRATA [43]	CTAS (Ours)
Agent capabilities	continuous/Gaussian	continuous/stochastic
Capability types	cumulative	cumulative/noncumulative
Task requirements	and	and/or
Scheduling	no	yes
Uncertainty control	limit variance	minimize CVaR

minimum value needed for each capability type. The work of [43] then models the problem as an optimal control process (called STRATA) where they penalize the time, misplaced capabilities, and the variance of the distribution. However, probability, expectation, or variance are not well-justified quantitative metrics in such an optimization problem and can result in problematic solutions. For instance, if the required capability of a task is matched precisely, it is reasonable to limit the variances within a small threshold. However, if the team’s capability surpasses the task requirement by a lot, larger variances are acceptable. As another example, optimizing an expected cost (average performance) can be problematic for safety-critical applications.

In our proposed model, we represent the agent capabilities as a vector of random distributions (not necessarily Gaussian) and the task requirements within a binary function of the team capabilities (defined in Sec. III). The task requirement is verified once the ‘sum capabilities’ of the team drive the binary function to one. Because there can be multiple ways to satisfy the ‘sum requirements’, the agent combination for a complex task is not enumerated but encoded implicitly. We then solve the task decomposition, assignment, and scheduling problem simultaneously, where we optimize the time, energy, and ‘uncertainty’. For the ‘uncertainty’, we choose to minimize the conditional value at risk (CVaR), which is a provably sensible measurement of the uncertainties in practical applications [44]. It is widely accepted by the finance community and appears with a growing frequency in recent robotic applications [45]–[49]. A graphical illustration of the definition of CVaR is shown in Fig. 3.

STRATA [43], [50] shares many similarities with our proposed approach, CTAS, including stochastic agent capability vectors, task requirements on the team’s sum capabilities, and graphical representations of the problem. Therefore, we choose STRATA as our baseline algorithm in one of the experiments in Sec. VI. However, STRATA falls in the area of CD-[ST-

MR-IA], where it assumes a schedule of the tasks is given, which simplifies one of the core components of such a multi-agent system. Meanwhile, our task model, represented using requirement functions, is more expressive. TABLE I provides a more detailed comparison between the two models.

III. ROUTING, SCHEDULING, AND RISK MINIMIZATION

In this section, we formally define the heterogeneous teaming problem with uncertain agent capabilities and task requirements. We describe the task requirement functions and agent capability vectors used to represent the task structure, organize them in a graphical model, and then encode the task allocation problem as a stochastic mixed-integer program whose objective jointly consists of time, energy, and risk cost.

A. Heterogeneous Teaming Problem Description

We simplify the graphical model in [16] for this work. Consider a set of agent species $V = \{v_1, \dots, v_{n_v}\}$, capability types $A = \{a_1, \dots, a_{n_a}\}$, and tasks $M = \{m_1, \dots, m_{n_m}\}$. Each agent specie $k \in V$ is associated with a non-negative capability vector $\mathbf{c}_k = [c_{ka_1}, \dots, c_{ka_{n_a}}]^\top$, where c_{ka} is a random variable with a known distribution, representing the uncertainty in agents' task capabilities. Each task $i \in M$ requires an agent team with appropriate capabilities that drives a task requirement function $\rho_i(\cdot)$ to 1.

A task requirement function is a binary function of similar structure as (1). The logical operators \geq , \wedge , and \vee are 'greater than', 'and', and 'or' that return 1 if their conditions are satisfied, and 0 otherwise. Note that there can be an arbitrary number of \wedge and \vee , theoretically. α_a is the capability a of the agent team. Depending on whether the capability is cumulative, we can compute α_a according to (2). An example of non-cumulative capabilities is the speed limit of a team. It equals the speed of the slowest moving agent in the team. γ_a reflects the task requirement on capability a , and is modeled as a random variable with a known distribution.

$$\begin{aligned} \rho_{m_1}(\alpha_{a_1}, \alpha_{a_2}, \dots) &= [(\alpha_{a_1} \geq \gamma_{a_1}) \vee (\alpha_{a_2} \geq \gamma_{a_2})] \\ &\wedge [\alpha_{a_3} \geq \gamma_{a_3}] \wedge [\alpha_{a_4} \geq \gamma_{a_4}] \end{aligned} \quad (1)$$

$$\alpha_a = \begin{cases} \sum_{k \in V_{m_1}} c_{ka}, & a \text{ is cumulative} \\ \min_{k \in V_{m_1}} c_{ka}, & a \text{ is non-cumulative} \end{cases} \quad \forall a \in A \quad (2)$$

The requirement to drive these functions to 1 could be satisfied with appropriate team formation planning. In our model, this requirement can be encoded as linear constraints [16]. In this representation, the only part that could introduce non-convexity is the logic \vee which takes the union of two feasible regions. Reducing the number of \vee is desired as it facilitates the optimization. Therefore, the representation is closer to convex than a simple enumeration of role decomposition.

With the stochasticity in task requirements and agent capabilities, the goal is to determine the optimal task schedule for a selected set of agents, such that the energy, time, and path constraints are satisfied, and the energy cost and the risk of task's non-completion are jointly minimized.

B. Routing Model

As shown in Fig. 4, we first define a directed graph $G = (N, E)$, with a set of vertices $N = S \cup U \cup M$ and edges E . $M = \{m_1, \dots, m_{n_m}\}$ is the set of the task nodes. $S = \{s_1, \dots, s_{n_v}\}$ and $U = \{u_1, \dots, u_{n_v}\}$ are the sets of start and terminal nodes respectively for each agent specie $v_i \in V$. Note that these nodes can represent the same or different physical locations in the real world.

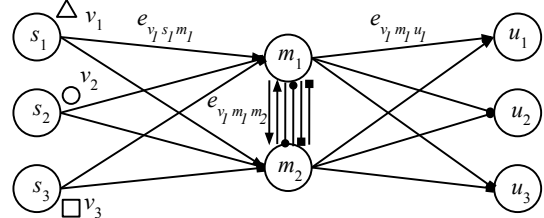


Fig. 4: Graphical model with 3 agent species and 2 tasks. The arrow type differentiates which agent specie an edge belongs to. Three edges are labeled as examples.

For each agent specie $v_k \in V$, there is an edge $e_{v_k s_k i}$ from the start node to the task node $i \in M$ and an edge $e_{v_k i u_k}$ from the task node $i \in M$ to its terminal node. For simplicity, we also use notation e_{ksi} for $e_{v_k s_k i}$ and e_{kiu} for $e_{v_k i u_k}$, as there will be no ambiguity for the start and terminal node once v_k is determined. Between each task node pair $i, j \in M$, there are edges e_{kij} and $e_{kji} \in E$ for all agent species $k \in V$.

Under this setting, the agents of specie v_k should start at s_k , follow the edges to visit a subset of task nodes (often together with other agents), and terminate at u_k . As a result, the agent numbers on the edges form a network flow from the start to the terminal nodes in the given graph G . Based on the graphical model G and all the above definitions, a mixed-integer program (MIP) can be formulated.

Compared to [16], two major differences in this work are that the nodes and edges are defined for agent species instead of individual agents (there are fewer copies of nodes and edges) and the agent number on an edge is now real instead of binary. These changes reduce the graph size and the number of variables and, therefore, decrease the computational cost of the planner. However, as the model does not specify variables for individual agents, the MIP outputs agent flow of each specie instead of path plans for individual agents. We will discuss algorithms for post-processing the agent flows to get routes for individual agents in Sec. V.

C. Risk Minimization Model

In this section, we discuss a MIP model that generates a schedule and agent team for each task, and the corresponding agent flow by minimizing the energy cost and the risk of task's non-completion. Here we provide common notations that will be used in TABLE II. Note that the variables are x_{kij} , y_{ki} , r_{kij} , r_{ki} , q_i , and g_{ki} .

1) *Variable Bounds*: The numbers of agents from specie $k \in V$ on an edge and at a task node are positive and real. Their helper variables are binary. The time and cumulative

Table II: Definition of the notations.

	Meaning
x_{kij}	The number of agents on edge e_{kij} with specie $k \in V$, where $i \in M \cup S$ and $j \in M \cup U$.
y_{ki}	The number of agents at task $i \in M$ with specie $k \in V$. = 1, if $x_{kij} \geq 1$, otherwise 0. (A helper variable indicating whether there are agents with specie k on that edge.)
r_{ki}	= 1, if $y_{ki} \geq 1$, otherwise 0. (A helper variable indicating whether there are agents with specie k at that task.)
q_i	The time that task $i \in M$ begins.
g_{ki}	The maximum cumulative energy that an agent of specie $k \in V$ has spent at node i . (A helper variable.)
b_{kij}	The deterministic energy cost to travel edge e_{kij} ($k \in V, i, j \in N$).
t_{kij}	The deterministic time to travel edge e_{kij} ($k \in V, i, j \in N$).
t_{ki}	The deterministic time for agent specie $k \in V$ to complete its part for task $i \in M$.
C_q	Time penalty coefficient.
C_{large}	A large constant number for the MIP.
B_k	The energy capacity of agent $k \in V$.
h_i	The conditional value at risk from task $i \in M$.

energy are positive.

$$x_{kij} \geq 0, y_{ki} \geq 0 \quad \forall i, j \in N, \forall k \in V \quad (3)$$

$$r_{kij}, r_{ki} \in \{0, 1\} \quad \forall i, j \in N, \forall k \in V \quad (4)$$

$$q_i \geq 0 \quad \forall i \in M \cup U, \quad q_i = 0 \quad \forall i \in S \quad (5)$$

$$g_{ki} \geq 0 \quad \forall i \in M \cup U, \quad g_{ki} = 0 \quad \forall i \in S \quad (6)$$

2) *Helper Variable Constraints*: (7) encodes the relationship between agent number variables $\{x_{kij}, y_{ki}\}$ and their helper variables $\{r_{kij}, r_{ki}\}$.

$$x_{kij} \geq r_{kij}, \quad x_{kij} \leq n_k \cdot r_{kij}, \quad \forall i, j \in N, \forall k \in V \quad (7)$$

$$y_{ki} \geq r_{ki}, \quad y_{ki} \leq n_k \cdot r_{ki}, \quad \forall i \in N, \forall k \in V \quad (8)$$

3) *Network flow constraints*: (9)-(11) are flow constraints that ensure the agent numbers are smaller than the upper bound, and that the incoming agent number at a node equals the outgoing number. (12) reflects the relationship that the number of agents at a node equals the sum of the agent flows from all incoming edges.

$$\sum_{i \in S \cup M} x_{kim} = \sum_{j \in U \cup M} x_{kmj} \quad \forall m \in M, \forall k \in V \quad (9)$$

$$\sum_{i \in M} x_{ksi} \leq n_k \quad \forall k \in V \quad (10)$$

$$y_{kj} \leq \sum_{i \in M} x_{ksi} \quad \forall j \in M, \forall k \in V \quad (11)$$

$$y_{kj} = \sum_{i \in S \cup M} x_{kij} \quad \forall j \in M, \forall k \in V \quad (12)$$

4) *Energy constraints*: (13) ensures that the maximum cumulative energy at node j is no smaller than the energy at its previous node i plus the edge cost in between. And because g_{ki} is the maximum cumulative energy of agent specie k at node i , (14) ensures the energy cost for an agent of specie k does not exceed its energy capacity B_k .

$$g_{ki} - g_{kj} + b_{kij} \leq B_{\text{large}}(1 - r_{kij}) \quad \forall i, j \in N, \forall k \in V \quad (13)$$

$$g_{ki} \leq B_k \quad \forall i \in N, \forall k \in V \quad (14)$$

These energy constraints are sufficient conditions as they assure the most costly path in the flow network of specie k is

within the capacity limit B_k . However, it is possible that the most costly path is not picked during the flow decomposition procedure (Sec. V). This is a compromise made by us along the process of improving the scalability of the model: we replace the variables for individual agents with variables for an entire agent specie. With the original variables for individual agents, necessary and sufficient energy constraints were easily imposed.

5) *Time constraints*: (15) is a scheduling constraint: for an agent, the time duration between two consecutive tasks should be larger than the service time at the previous task plus the travel time. Since this duration constraint is effective for all agents in a team, it gives all the agents in the team enough time to arrive before the current task starts.

$$q_i - q_j + t_{kij} + t_{ki} \leq C_{\text{large}}(1 - r_{kij}) \quad \forall i, j \in N, \forall k \in V \quad (15)$$

6) *Task requirement constraints*: Though the task requirements and the agents' task capabilities are stochastic, we can add a deterministic constraint that requires the teams' expected capabilities to satisfy the task requirement by driving the requirement function to 1. Note that for non-cumulative capabilities, we replace the \sum in (16) with min.

$$1 = \rho_i(\sum_{k \in V} E\{c_{ka_1}\}y_{ki}, \sum_{k \in V} E\{c_{ka_2}\}y_{ki}, \dots) \quad \forall i \in M \quad (16)$$

7) *Objective function*: In the objective function (17), we want to minimize a weighted combination of the energy cost, task time, and the conditional value at risk of the task's non-completion. Here, the task m_1 in (1) is used as an example to illustrate the math definition of the risk of a task h_i . m_1 requires the capability of a_1-a_4 . Assuming these requirements on these capabilities are independently placed, the total risk is the sum of the risk of each requirement. Take a_3 in (1) as an example, where the task requires the team capability larger than a threshold, $\alpha_{a_3} \geq r_{a_3}$. Since both α_{a_3} and γ_{a_3} are stochastic, in order to maximize the probability $P(\alpha_{a_3} \geq \gamma_{a_3})$, we instead, minimize the CVaR of $\gamma_{a_3} - \alpha_{a_3}$. Let the function $\eta_\beta(\cdot)$ be the CVaR of a random variable with probability level β . The risk $h_{m_1 a_3}$ can be computed according to 20 or 19 depending on whether a_3 is cumulative or not.

$$\min C_e \sum_{k \in V} \sum_{i, j \in N} b_{kij} \cdot x_{kij} + C_q \sum_{i \in U} q_i + C_h \sum_{i \in M} h_i \quad (17)$$

$$h_{m_1} = h_{m_1 a_1} + h_{m_1 a_2} + h_{m_1 a_3} + h_{m_1 a_4} \quad (18)$$

$$h_{m_1 a_3} = \max_{k \in V \text{ s.t. } r_{k m_1} = 1} \eta_\beta(-c_{ka_3} + \gamma_{a_3}) \quad (19)$$

$$h_{m_1 a_3} = \eta_\beta(-\sum_{k \in V} c_{ka_3} \cdot y_{km_1} + \gamma_{a_3}) \quad (20)$$

Given the uncertainty in the capabilities, the objective function (12), together with the deterministic task requirement constraint (16), tries to maximize the probability of task success at a low energy and time cost.

D. Sample Average Approximation (SAA)

Solving the optimization specified by (3)-(20) requires dealing with stochasticity and nonlinearity. In this section, we

show how to convert this stochastic mixed-integer nonlinear program (MINLP) to a deterministic mixed-integer linear program (MILP).

Notice that the $E\{c_{ka}\}$ in (16) and the $\eta_\beta(-c_{ka_3} + \gamma_{a_3})$ in (19) do not involve decision variables, these can be computed prior to the optimization, given the distribution of the c 's and γ 's. The stochasticity is eliminated by the expectation and risk function. The deterministic task requirements (16) can then be represented with a set of linear constraints according to [16]. (19) can also be represented as a linear constraint as in (21).

$$h_{m_1 a_3} \geq \eta_\beta(-c_{ka_3} + \gamma_{a_3}) \cdot r_{km_1} \quad k \in V \quad (21)$$

The only non-linearity is in (20) due to the function $\eta_\beta(\cdot)$ and the decision variable y_{km_1} . However, we can linearize it using the sample average approximation algorithm. Suppose we can represent the random distribution c_{ka_3} and γ_{a_3} by samples $c_{ka_3}^{(\xi)}$ and $\gamma_{a_3}^{(\xi)}$ ($\xi = 1, \dots, n_\xi$), respectively. Then we can approximate (20) with a linear equation (22) according to [51]. The approximation converges at the rate of $\mathcal{O}(n_\xi^{-1/2})$ [52].

$$h_{m_1 a_3} = \lambda_{m_1 a_3} + 1/n_\xi (1 - \beta) \cdot \sum_{\xi=1}^{n_\xi} \left[- \sum_{k \in V} c_{ka_3}^{(\xi)} \cdot y_{km_1} + \gamma_{a_3}^{(\xi)} - \lambda_{m_1 a_3} \right]^+ \quad (22)$$

$$[x]^+ = \begin{cases} x, & x > 0 \\ 0, & x \leq 0 \end{cases} \quad (23)$$

Finally, the piece-wise linear function in (22) can be represented as linear constraints in (24)-(26).

$$h_{m_1 a_3} = \lambda_{m_1 a_3} + \frac{1}{n_\xi(1 - \beta)} \sum_{\xi=1}^{n_\xi} w_{m_1 a_3}^{(\xi)} \quad (24)$$

$$w_{m_1 a_3}^{(\xi)} \geq - \sum_{k \in V} c_{ka_3}^{(\xi)} \cdot y_{km_1} + \gamma_{a_3}^{(\xi)} - \lambda_{m_1 a_3} \quad (25)$$

$$w_{m_1 a_3}^{(\xi)} \geq 0 \quad (26)$$

IV. THE L-SHAPED ALGORITHM

In the previous section, we formulate the stochastic heterogeneous teaming problem as an MINLP optimization and approximate it as a MILP using sample average approximation. However, the number of variables and constraints in the linear program is a function of the sample number n_ξ . When the sample number dominates, the size of the linear program is roughly $\mathcal{O}(n_\xi)$, and the computation complexity is $\mathcal{O}(n_\xi^2)$. Therefore, when the sample number is large, solving the teaming problem through MILP can still be expensive.

Due to the specific structure of the large MILP described in Sec. III, we can explore the sparsity and decouple the large problem into a two-stage linear program. This method is called the L-shaped algorithm [53], which returns the same optimal solution but reduces the computation cost from $\mathcal{O}(n_\xi^2)$ approximately to $\mathcal{O}(n_\xi)$ with a larger constant coefficient empirically.

The general structure of the algorithm is summarized in Algorithm 1. At the first stage, the algorithm solves a fixed-sized mixed-integer linear program (the size is not a function

Algorithm 1: L-shaped algorithm for the model.

```

1 Input: The unsolved optimization problem (27)-(30)
2 for  $m \in M$  and  $a \in A$  do
3    $L_{ma} = 0$ 
4 while True do
5   Solve the first stage problem (27)-(31) and let
6    $(y_{v_1 m}^{[p]}, \dots, y_{v_{n_v} m}^{[p]}, \lambda_{ma}^{[p]}, \theta_{ma}^{[p]}, x_{kij}^{[p]})$  be the solution.
7   flag = True
8   for  $m \in M$  and  $a \in A$  do
9     //  $L_{ma}$  is abbreviated to  $L$  in the following lines.
10    for  $\xi = 1 : n_\xi$  do
11      Solve the second stage problem (32)-(34) and let
12       $\pi_{ma}^{(\xi)[p]}$  be the Lagrangian multiplier associated
13      with the solution  $w_{ma}^{(\xi)[p]}$ .
14      Calculate  $D_{ma}^{[L]}$  and  $d_{ma}^{[L]}$  according to (35)-(36).
15      if  $D_{ma}^{[L]}[y_{v_1 m}^{[p]}, \dots, y_{v_{n_v} m}^{[p]}, \lambda_{ma}^{[p]}]^\top + \theta_{ma}^{[p]} < d_{ma}^{[L]}$ 
16        then
17          flag = False
18           $L = L + 1$ 
19          Add the cut
20           $D_{ma}^{[L]}[y_{v_1 m}, \dots, y_{v_{n_v} m}, \lambda_{ma}]^\top + \theta_{ma} \geq d^{[L]}$ 
21        if flag then
22          return the solution  $x_{kij}^{[p]}$  // Optimality obtained.

```

of n_ξ). At the second stage, it solves n_ξ small linear programs and then adds cuts to the first stage program according to the second-stage solutions. The two stage is iterated until convergence.

The first stage problem in the algorithm is (27)-(31). Note that equations (27)-(29) are the same as (17), (19), and (21), but are copied here for clarity. If capability a_3 is non-cumulative, then $h_{m_1 a_3}$ is calculated according to (29). If a_3 is cumulative, the large linear program described in (24)-(26) is replaced with (30)-(31). $\theta_{m_1 a_3}$ is a lower bound for $\sum_{\xi=1}^{n_\xi} w_{m_1 a_3}^{(\xi)}$ in (25), and is tightened iteratively with cuts in (31) obtained from the second stage. Note that (29)-(31) and the following second stage problem as a whole is only an example for calculating $h_{m_1 a_3}$. Similar operations are applied to compute all other h_{ma} 's where $m \in M$ and $a \in A$.

$$\min C_e \sum_{k \in V} \sum_{i,j \in N} b_{kij} \cdot x_{kij} + C_q \sum_{i \in U} q_i + C_h \sum_{i \in M} h_i \quad (27)$$

s.t. (3)-(16) and

$$h_{m_1} = h_{m_1 a_1} + h_{m_1 a_2} + h_{m_1 a_3} + h_{m_1 a_4} \quad (28)$$

$$h_{m_1 a_3} \geq \eta_\beta(-c_{ka_3} + \gamma_{a_3}) \cdot r_{km_1} \quad k \in V \quad (29)$$

$$h_{m_1 a_3} = \lambda_{m_1 a_3} + \frac{1}{n_\xi(1 - \beta)} \theta_{m_1 a_3} \quad (30)$$

$$D_{m_1 a_3}^{[\ell]}[y_{v_1 m_1}, \dots, y_{v_{n_v} m_1}, \lambda_{m_1 a_3}]^\top + \theta_{m_1 a_3} \geq d^{[\ell]} \quad \forall \ell = 1, \dots, L \quad (31)$$

The second stage problem is described in (32)-(34): once y_{km_1} and $\lambda_{m_1 a_3}$ are determined in the first stage, the large linear program in (24)-(26) can be decoupled into n_ξ small linear programs with analytic solutions.

$$\min w_{m_1 a_3}^{(\xi)} \quad (32)$$

$$\text{s.t. } w_{m_1 a_3}^{(\xi)} \geq - \sum_{k \in V} c_{ka_3}^{(\xi)} \cdot y_{km_1}^{[p]} + \gamma_{a_3}^{(\xi)} - \lambda_{m_1 a_3}^{[p]} \quad (33)$$

$$w_{m_1 a_3}^{(\xi)} \geq 0 \quad (34)$$

An additional optimality cut can be added in (31) according to the Lagrangian multipliers (simplex multipliers) $\pi_{m_1 a_3}^{(\xi)[p]}$ associated with the second stage solutions. The parameters of the cuts are calculated as follows in (35)-(36).

$$D_{m_1 a_3}^{[L]} = \sum_{\xi=1}^{n_{\xi}} \pi_{m_1 a_3}^{(\xi)[p]} [c_{v_1 a_3}, \dots, c_{v_{n_v} a_3}, 1] \quad (35)$$

$$d_{m_1 a_3}^{[L]} = \sum_{\xi=1}^{n_{\xi}} \pi_{m_1 a_3}^{(\xi)[p]} \cdot \gamma_{a_3}^{(\xi)} \quad (36)$$

The Lagrangian multipliers $\pi_{m_1 a_3}^{(\xi)[p]}$ are obtained by solving the second stage dual problem (37)-(38), and the solutions are shown in (39).

$$\max \left(- \sum_{k \in V} c_{ka_3}^{(\xi)} \cdot y_{km_1}^{[p]} + \gamma_{a_3}^{(\xi)} - \lambda_{m_1 a_3}^{[p]} \right) \cdot \pi_{m_1 a_3}^{(\xi)} \quad (37)$$

$$\text{s.t. } 0 \leq \pi_{m_1 a_3}^{(\xi)} \leq 1 \quad (38)$$

$$\pi_{m_1 a_3}^{(\xi)[p]} = \begin{cases} 0, & - \sum_{k \in V} c_{ka_3}^{(\xi)} \cdot y_{km_1}^{[p]} + \gamma_{a_3}^{(\xi)} - \lambda_{m_1 a_3}^{[p]} < 0 \\ 1, & \text{otherwise} \end{cases} \quad (39)$$

V. DECOMPOSE AGENT FLOWS INTO PATHS

Solving the teaming problem in Sec. III using the algorithm in Sec. IV provides the optimal solutions to $x_{kij}, \forall k \in V, \forall i, j \in N$, i.e. the flows of different agent species. An example is shown in Fig. 5a, where the flow values are not necessarily integer. This section discusses an optimal algorithm to extract a routing plan for each individual agent from the agent flows.

Formally, A flow network is a graph $G(N = S \cup M \cup U, E)$ with a function $f(\cdot) : E \rightarrow \mathbb{R}$, where S , M , U , and E denotes the set of start nodes, intermediate nodes, terminal nodes, and directed edges, respectively. For a node $m \in M$, suppose the incoming and outgoing edge sets are E_m^{in} and E_m^{out} , respectively. Then, the function $f(\cdot)$ should satisfy (40). In this section, the flow function $f(e_{kij}) = x_{kij}$ indicates the agent number on an edge.

$$\sum_{e \in E_m^{\text{in}}} f(e) = \sum_{e \in E_m^{\text{out}}} f(e) \quad \forall m \in M \quad (40)$$

A. Problem Description

Because the agent numbers cannot be fractional, we need to round off these flows to integers and then pick individual agents and their paths to cover the flow. As an example, the flow network of v_1 is extracted and rounded off in Fig. 5b. Then, in Fig. 5c, three individual agent paths with flows of 1 on the path edges are selected such that the sum flow of the three paths equals the rounded integer network flow in Fig. 5b. Note that in order to maintain the task requirements

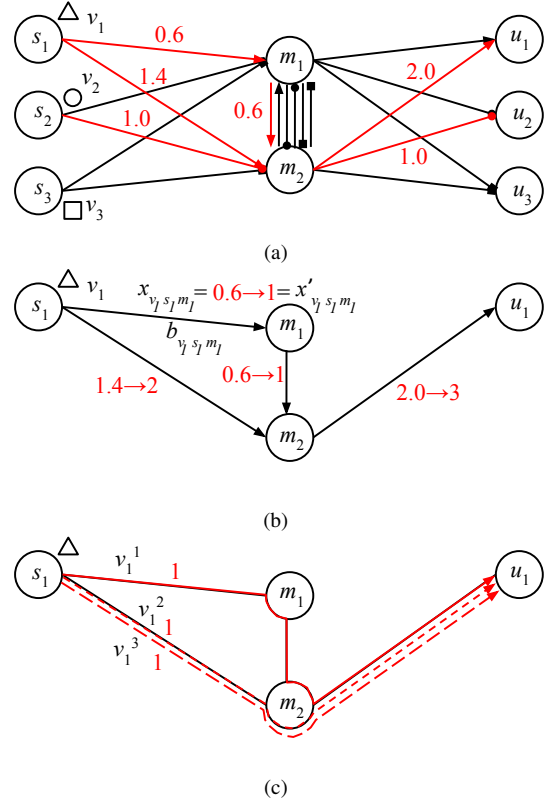


Fig. 5: Decompose a flow into paths. The x 's are the flow on an edge, with the red numbers an example of the actual value. The b 's are the energy cost of the edge. (a) Resulted agent flows. (b) The flow of agent specie v_1 . (c) The path cover of agents specie v_1 using three individuals.

in equation (1), we have to round up a fractional flow rather than round it to the nearest integer. This rounding up results in a suboptimal but still feasible solution.

The rounding up process has to maintain the flow constraints: for all of the nodes, the incoming flow equals the outgoing flow. A naive rounding up might break the flow constraint. Take the node m_3 in Fig. 6a as an example: naively rounding up the flows on an edge will result in 2 incoming agents but 3 outgoing agents.

When the flow constraints are maintained, there can still be multiple rounding off choices. For instance, the Fig. 6b-c are both valid ways to round off the flow in Fig. 6a. However, the energy cost of the flow in Fig. 6c is higher. Therefore, the optimal rounding up will need to maintain the flow constraint and introduce the lowest additional energy cost.

After rounding off the flow to integers, there are multiple choices to assign individual agent paths. We call this ‘cover a flow with paths’. For example, the flow in Fig. 6b can be covered with the 3 agent routes either in Fig. 7a or Fig. 7b. Though the sum energy costs are the equivalent, the energy cost of the three paths in the two choices are $\{20, 20, 20\}$ and $\{20, 24, 16\}$, respectively. The choice affects the behavior of an individual agent. Here, we prefer the former cover, because the energy costs of individual agents are more evenly distributed and the maximum energy cost of an individual agent is smaller. We define the optimal flow cover as the set of paths that minimizes maximum individual energy cost.

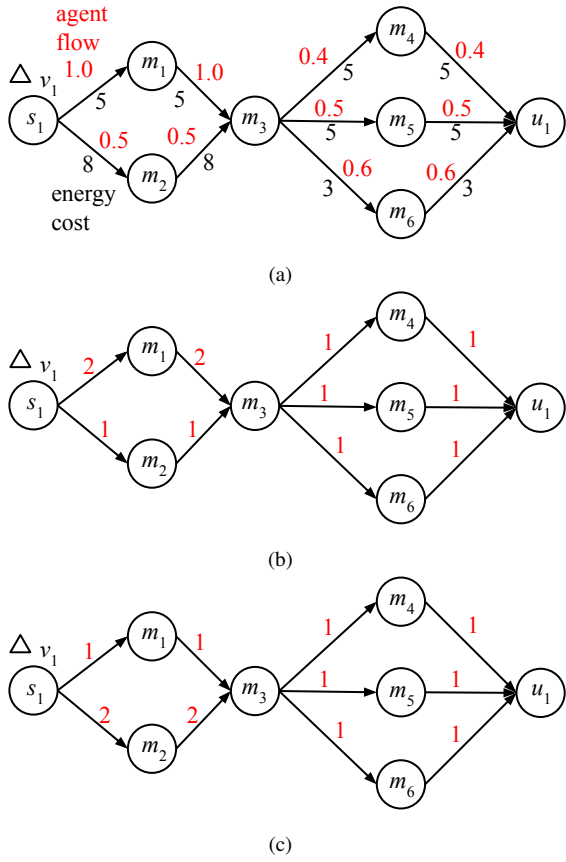


Fig. 6: Round up the flow of agent specie v_1 . The red number is the agent flow on an edge. The black number below an edge are the energy cost of the edge. (a) The original flow with real numbers. (b) Round up choice 1. (c) Round up choice 2.

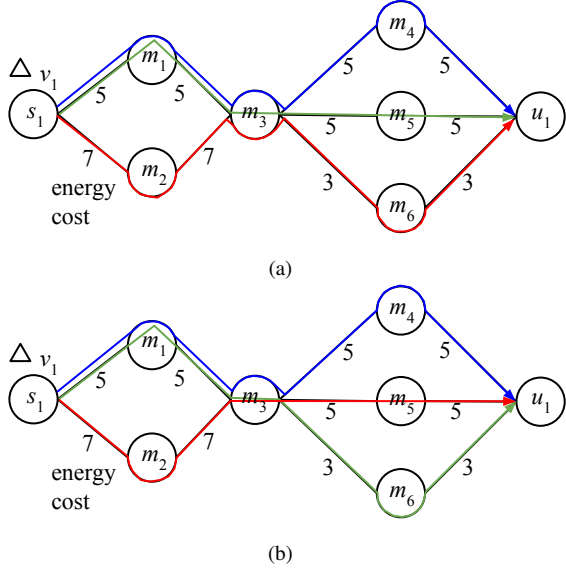


Fig. 7: Cover the agent flow in Fig. 6b with 3 paths. The black number below an edge are the energy cost of the edge. There are two choices with different individual costs. (a) Choice 1. (b) Choice 2.

B. The Minimum Energy Cost Rounding Up

According to the previous section, optimally decomposing a real-numbered agent flow into individual agent routes can be divided into two steps: rounding up to an integer flow with the lowest additional cost and covering the integer flow with low-

cost individual paths. This section discusses a linear program to round the real-numbered flow with minimum additional energy cost.

See Fig. 5b as an example, suppose the flow output from the MIP model in Sec. III for agent specie $k \in V$ is x_{kij} on edge e_{kij} . Let the integer flow after the rounding off process be x'_{kij} . Then, the linear program in (41)-(44) will return an integer flow network with minimum energy cost. The objective function (41) penalizes the energy cost. (42) ensures the rounding off is happening upward, where $\lceil x_{kij} \rceil$ denotes the smallest integer larger than x_{kij} . The network flow constraint (44) should be maintained during the optimization. S , U , and M are the set of start, terminal, and task nodes respectively. $N = S \cup M \cup U$.

$$\min \sum_{i,j \in N} b_{kij} \cdot x'_{kij} \quad (41)$$

$$\text{s.t. } x'_{kij} \geq \lceil x_{kij} \rceil \quad \forall x_{kij} > 0 \quad (42)$$

$$x'_{kij} = 0 \quad \forall x_{kij} = 0 \quad (43)$$

$$\sum_{i \in S \cup M} x_{kim} = \sum_{j \in U \cup M} x_{kmj} \quad \forall m \in M \quad (44)$$

Note that there is no explicit integer constraint here to assure that x'_{kij} is integer. However, if this linear program is solved using Simplex-based algorithms, the solutions to x'_{kij} are guaranteed to be integers. Because of this, the minimum energy rounding off problem could be solved in polynomial time through a linear program (instead of an integer linear program).

A brief proof that solutions will be integers: since this round up problem falls in the category of minimum cost flow problems, if converted to the form $\min \mathbf{c}^T \mathbf{x}$ with $A\mathbf{x} \leq \mathbf{b}$, $\mathbf{x} \geq 0$, the A matrix will be totally unimodular [54]. Meanwhile, the entries in \mathbf{b} will be integers. Because of the total unimodularity, all extreme points (possible solutions) of the polytope defined by the linear constraints, $A\mathbf{x} \leq \mathbf{b}$ and $\mathbf{x} \geq 0$, will be integers. And an integer solution is guaranteed if Simplex-based algorithms are applied as it searches through the extreme points.

C. The Minimum Max-Energy Flow Cover

After the rounding off, we get the integer flows x'_{kij} in Fig. 5b, the next step is to decompose this integer flow into individual agent paths in Fig. 5c. By summing up the out going flow at the start node, we are able to get the needed number of agents from specie $k \in V$, denoted as n'_k . Then we compose n'_k graphs as in Fig. 8 for the n'_k agent individuals for $k \in V$.

We can formalize an integer linear program (ILP) to find the routes for all the individual agents, such that the maximum individual energy cost is minimized and the unit agent flow on these paths sums up to the original network flow in Fig. 5b. In the following ILP, the objective (45) penalizes the maximum energy cost of an individual agent. (46) ensures that the result agent flows in Fig. 8 sum up to Fig. 5b. (47) is the network constraint. (48) requires that in each subgraph in Fig. 8, there is only one agent.

$$\min_{x_{kij}^l} \max_l \sum_{i,j \in N} b_{kij} \cdot x_{kij}^l \quad (45)$$

$$\text{s.t. } \sum_{l=1}^{n'_k} x_{kij}^l = x'_{kij} \quad \forall i, j \in N \quad (46)$$

$$\sum_{i \in N} x_{kim}^l = \sum_{j \in N} x_{kmj}^l \quad \forall m \in M, \quad \forall l = 1, \dots, n'_k \quad (47)$$

$$\sum_{i \in M} x_{ksi}^l = 1 \quad \forall l = 1, \dots, n'_k \quad (48)$$

$$x_{kij}^l \in 0, 1 \quad \forall i, j \in N, \quad \forall l = 1, \dots, n'_k \quad (49)$$

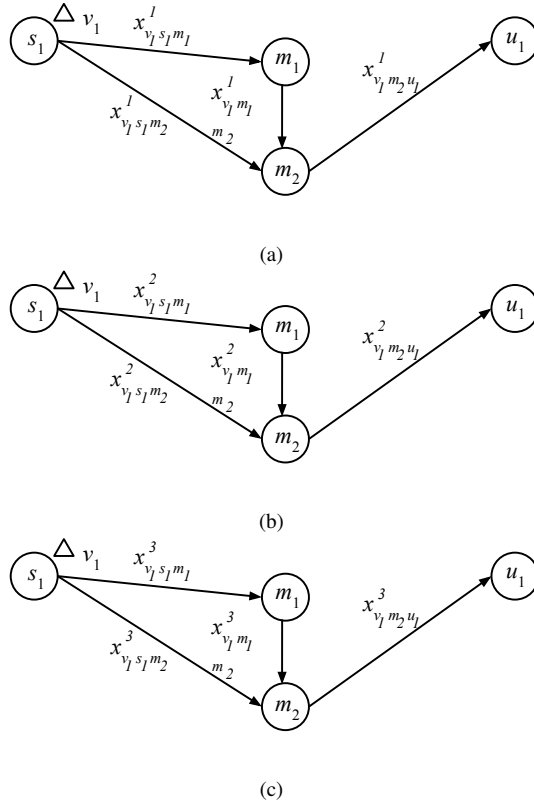


Fig. 8: Graphical model for the minimum max-energy flow cover problem for agent specie v_1 . The x 's are the flow on an edge. (a)(b)(c) are the flow networks for the three agent individuals of specie v_1 .

VI. EXPERIMENTS AND RESULTS

In this section, we first initialize randomized flow networks to test the model of decomposing agent flows, and then use two practical applications to show the robustness and generalizability of the proposed risk minimization model. All computations were done on a laptop with Intel i7-7660U CPU (2.50GHz).

A. Decompose Agent Flows into Paths

1) *Setup and Test Cases:* An agent flow network with random connections is initialized, and the flow and unit cost of each edge are sampled from uniform random distributions. The hyper-parameters are the maximum flow on an edge and

Table III: The computational cost of the flow decomposition. ‘Task’ is the number of tasks, which equals to the number of nodes in the flow network. ‘Flow’ is the sum agent flow number from the start to the terminal node and ‘int flow’ is the value after rounding off. The ‘round time’ and ‘cover time’ are the time used to solve the rounding and cover problems, and the units are both seconds.

Case	Task	Edge	Flow	Int flow	Round time	Cover time
1	5	15	155.56	161	0.001	0.69
2	10	29	24.89	33	0.001	0.15
3	10	27	212.64	220	0.005	1.28
4	35	101	139.40	173	0.002	10.58
5	70	211	148.26	234	0.001	142.58

the node number of the network. The optimization models in Sec. V are then applied to the initialized random flow network to solve the minimum energy cost rounding up and minimum max-energy flow cover problems. The computational costs and the optimality of the solutions are then evaluated under different sizes of test cases.

2) *Result and Discussion:* Different sizes of flow decomposition problems are solved, and the computational costs of the two steps are listed in TABLE III. The size of the rounding and cover problems are proportional to edge number and edge number \times sum integer flow, respectively. For the cases shown in TABLE III, the rounding steps can be completed within several milliseconds. The rounding process scales well because the linear program can be solved in polynomial time. The cover step involves solving an integer linear program, which does not scale well generally with the problem size. The largest test case shown in the table involves 70 tasks and 234 agents, much larger than the typical teaming problem sizes that the risk minimization model will be applied to. Therefore, the flow decomposition part will not be the bottleneck of the overall teaming planner.

Though there are no explicit integer constraints in the rounding up model in Sec. V-B, we provided a proof in Sec. V-B that showed that the solutions would be integers, and the results support it. As an example, the rounding up solution of case 1 is shown in Fig. 9, where we can see that the agent flow on each edge is rounded up to an integer, while the overall network flow constraint is maintained. For instance, the 13.41 on edge (S, 1) is rounded to 15 instead of 14 in order to maintain the flow constraint.

B. Capture the Flag

In this section, we apply the risk minimization model in Sec. III to a team of agents in a capture the flag game setting and compare the team performance against the baseline (STRATA [43]) in a simulation environment (Fig. 10). The goal of this simulation is to evaluate and demonstrate the performance of the task assignment component of our framework. The number of wins is used as the metric for the task performance.

1) *Game Setup, Baseline, and Metrics:* The blue and green teams contain 12 heterogeneous agents initialized at random locations within their own sides. The overall goal is to win the game by taking the flag of the other side back. The 12 agents are from 4 species (3 individuals for each species). These species are with different speed, viewing distance, health, and ammunition capabilities (TABLE IV). The specific values in

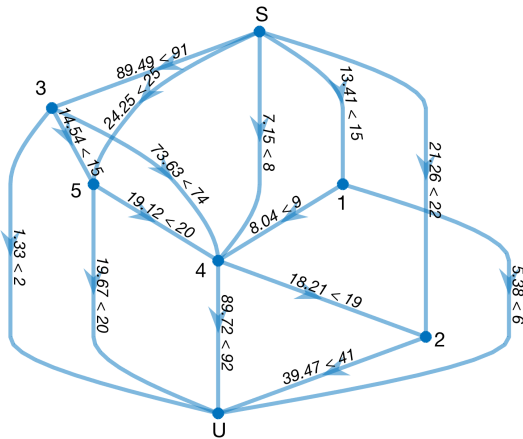


Fig. 9: Flow round up result (5 task nodes, 15 edges). There are two numbers on each edge, indicating the agent flows before and after the round up process. This example corresponds to case 1 in TABLE III.

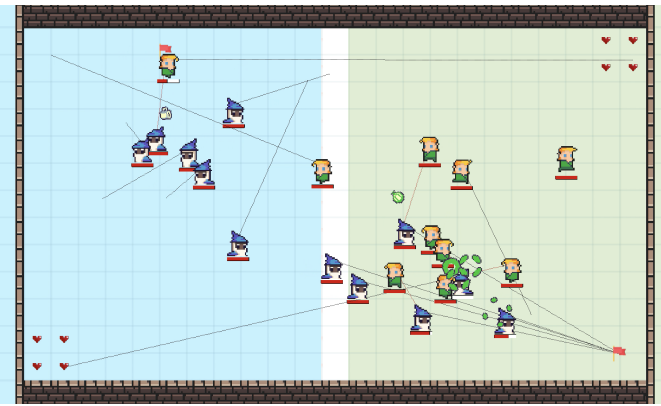


Fig. 10: Capture the flag setup. Each small square tile is 1×1 unit length. A line points to the current target of the corresponding agent.

the table are set according to the baseline paper [43]. Among these capabilities, the first two are noncumulative, while the last two are cumulative.

Each agent can play a role in one of the 3 tasks in TABLE V and will disappear when its health reaches zero. The adversarial elements of the game are not explicitly modeled, and the focus is to assign tasks such that the requirements are fulfilled while overall time and energy costs are considered in the trade-off. Therefore, the agents follow predefined behaviors once their tasks are determined.

STRATA [43] is chosen as the baseline of this work because its model makes use of similar concepts like agents, species, capability vectors, and task requirements specified by capabilities. While STRATA has no ability to output a schedule of the tasks, the tasks in this game are all ‘life-long’ tasks, and in such a setting, there is no scheduling aspect, and CTAS reduces to an instantaneous task assignment, tackling the same type of problem as STRATA does. Therefore, this game simulation will give us a fair comparison between STRATA and the task assignment component of our work under the metric of number of wins. Apart from STRATA, we also compare our model to a random task assignment mechanism where an agent is randomly assigned a task.

All games are played with two teams using different assignment models. The metric used in this simulation is the

number of wins in 500 games, which reveals the relative task assignment performances. A win is either a team taking back the other side’s flag or defeating all enemies using bullets. A draw happens when all agents from both sides decide to defend and no longer attack, or no team wins the game within 120 seconds.

Both STRATA and our model need task requirements specified as capability distributions. For the three tasks, the agents are programmed to switch to heal automatically when their health is lower than a threshold, and the required capabilities of the attack and defend tasks are listed in TABLE VI. The specific numbers are manually decided to reflect the following requirements: the attack task needs agents with higher speed and health to capture the flag, while the defend task needs agents with higher viewing distance and ammunition to detect and defeat the opposing team.

Table IV: Capability distributions of the four agent species. μ_i and σ_i^2 ($i = 1, \dots, 4$) are the mean and variance of the capability distributions of speed, viewing distance, health, and ammunition.

Specie	μ_1	μ_2	μ_3	μ_4	σ_1^2	σ_2^2	σ_3^2	σ_4^2
1	1.5	2	90	40	0.35	0.1	10	3
2	1.5	4	60	40	0.35	0.1	10	3
3	3	2	80	30	0.35	0.1	10	3
4	3	4	350	30	0.35	0.1	10	3

Table V: General task descriptions.

Task	Description
Attack	Try to capture the flag of the other side
Defend	Apply a defense mode to defeat opposing team members
Heal	Use hearts to apply healing powers

Table VI: Task requirements specified as capabilities distributions. The 1131 is 65% of the expected total initial health of the 12 agents, and 231 is 55% of the expected total ammunition.

	Speed	View	Health	Ammunition
Attack	≥ 2		≥ 1131 (65%)	
Defend		≥ 1		≥ 231 (55%)

2) *Results:* Based on all the settings described in the above section, we developed a simulation environment in C++. A screenshot is shown in Fig. 10. The three task assignment models, random, baseline, and CTAS, are linked with the simulation environment. During the simulation, the mean time for the baseline and CTAS to optimize and output an assignment are 0.43 and 0.04 seconds, respectively.

The relative performances of the models are shown in Fig. 11. As can be seen from Fig. 11, CTAS results in a higher win rate as compared to the baseline or random selection methods.

The number of agents assigned to attack, grouped by species, are shown in Fig. 12. According to the figure, CTAS is more likely to use specie 4 and does not use species 1 and 2. The baseline methods shows a similar trend of preferring specie 4 over the other species. This preference is logical since specie 4 contains attributes of high speed and health, which are more suitable for the attack task than other species’ attribute distributions (particularly specie 1 and 2). Though the

baseline claims to be able to consider noncumulative capability through thresholding, it lacks an explicit mechanism to prevent incompetent agents from joining a task. For instance, though specie 1 and 2 are not competent for the attack task due to their low speed, they are still allowed to conduct the task and contribute to other required capabilities such as health. However, this is not a good choice as there exist other agents that satisfy both the speed and health requirements of the attack task. Another possible factor contributing to CTAS's improved performance is that the CTAS algorithm directly minimizes the CVaR metric, which ensures enough task required capabilities, whereas the baseline focuses on matching the expected requirements and penalizing variance of the assigned capability distributions.

In conclusion, through the comparison, our framework demonstrates superior task assignment performance against the baseline algorithm, and the task assignment patterns in Fig. 12 support this performance result.

	Blue Wins	Draws	Green Wins
Random vs. Baseline	194	22	284
Random vs. CTAS	151	25	324
Baseline vs. CTAS	203	4	293

Fig. 11: Relative performances of random task assignment, baseline, and CTAS. Each row shows the mean result from ten 500 capture the flag games.

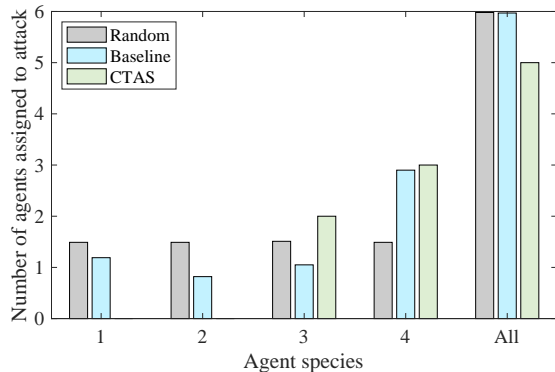


Fig. 12: Agent assigned to attack.

C. Robotic Services during a Pandemic

In this section, we demonstrate how the CTAS framework can be applied to a real-world example and show the full task assignment and scheduling components of the framework. A different application than the capture-the-flag game in Sec. VI-B also supports the claimed generalizability of CTAS. The energy cost and probability of success will be used to evaluate the optimality of the plans generated by the framework. The optimality gap given limited time for the optimization will be used to evaluate the scalability of the framework.

The COVID-19 pandemic has strongly affected society, industry, and daily lives around the world. On the other hand, it stimulated robotic applications in hospitals, public

health, transportation, and manufacturing to reduce physical human interaction [55]. Autonomous and teleoperated drones, vehicles, humanoids, and manufacturing robots are utilized to handle or assist disinfection and cleansing, patient diagnosis and treatment, medical triage, quarantine enforcement, delivery, and medical kit manufacturing [55]–[57]. A pandemic response or post-pandemic recovery mission requires all of these robots to form teams, cooperate, and handle tasks together. In such a situation, it is important for the task assignment and scheduling framework to capture the agents' heterogeneity, quickly adapt to changes in the task setup, and consider the uncertainty due to the lack of information. Therefore, this section uses this pandemic robotic services coordination as an example and shows how our framework considers the heterogeneity and uncertainty in a practical problem.

To the best of our knowledge, no existing framework focuses on the same HTP as this work (though there are models solving some components of this problem in the context of vehicle routing and task allocation). Therefore, we compare the current model to the one in our previous work [16].

1) *Experiment Setup and Model Description*: Consider pandemic robotic services in a city environment consisting of multiple delivery, disinfection, test, and treatment sub-tasks that require one or multiple robots to complete. The task requirements and agent capabilities are uncertain. We choose to include 8 types of tasks and 7 agent species in this illustration based on our investigation. These chosen tasks are a subset of the tasks we mentioned above at the beginning of this section. Note that some of the agents need a human operator.

Applying the CTAS model to describe the problem of the pandemic robotic services, we first define 9 capability types according to the chosen tasks and agents in TABLE VII.

The 7 agent species and their capabilities are defined in TABLE VIII, according to real-world references [55]. The agent capabilities are random variables and are assumed Gaussian distributed in this example.

The 8 task types and their required capabilities are listed in TABLE IX. Apart from the ones with self-explanatory names, we add further explanation to the following tasks. m_3 medical kit delivery: the team should be equipped with freezers; m_4 contaminants removal: remove contaminated materials and then disinfect the location; m_5 open area disinfection: perceive and locate a contaminated area to conduct contaminants removal and disinfection; m_6 quarantine enforcement: perceive, locate, carry materials to, disinfect a contaminated area, and then place signals and barricades to enforce a quarantine in the area. These tasks are distributed in a city. An example of 16 tasks (two tasks from each type) is shown in Fig. 18a. The agents start from the base, which, in practice, can be a hospital.

We use the M3500 data set [58] as the city's road map in this illustration. Suppose we can receive information about the safe and contaminated regions. For instance, if a location in the city map is exposed to viral contamination, we can then regard the neighborhood as dangerous and set the cost to travel within that area as high. Based on such an idea, a cost map indicating the viral exposure in an area can be

Table VII: Definitions of the capability types.

Definition
a_1 Fly
a_2 Equipped with a freezer
a_3 Deliver materials
a_4 Conduct perception
a_5 Remove and collect harmful materials
a_6 Conduct viral test
a_7 Physically interact and conduct treatment
a_8 Spray disinfectant
a_9 Place signals and barricades to conduct quarantine enforcement

Table VIII: Agent capabilities. The values are expectations of the random distributions, and the standard deviations are 10% of the expectations.

Agent specie	a_1	a_2	a_3	a_4	a_5	a_6	a_7	a_8	a_9
v_1 : Quadcopter	1	1	1			1			
v_2 : Vehicle			1						2
v_3 : Vehicle (freezer)		1	1						
v_4 : Vehicle (contaminants)				1			1		
v_5 : Guidance robot				1					5
v_6 : Test robot					1				
v_7 : Treatment robot					1	1			

modeled as a Gaussian process [59] where we use a set of known Gaussian distributions to infer a collection of correlated Gaussian distributions. For the example city map in Fig. 18a, we randomly choose 6 contaminated and 6 proven-safe regions as samples and learn a viral exposure map. The blue and red regions have low and high cost, respectively, while the white regions have less information, high ambivalence, and are assigned a medium cost. Based on this, we compute a viral-exposure-based travel cost between the tasks and regard it as the energy cost for the edges in the diagram in Fig. 4.

We choose the agents and tasks from their types in TABLES VIII and IX and compose 32 mission cases of different sizes where the agent numbers, task numbers, and the coefficient γ are chosen from $\{21, 70, 140\}$, $\{16, 24, 32, 40\}$, and $\{1, 3, 5, 10\}$, respectively. As an example, the smallest case consists of 21 agents and 16 tasks, it means there are 3 agents from each agent specie v_1 to v_7 . And the 16 tasks in the examples are distributed according to rule: m_1 and m_9 are task type 1 in TABLE IX, m_2 and m_{10} are type 2, ..., m_8 and m_{16} are type 8. Note that m_i and m_{i+8} have the same capability requirements, but are at different location.

Based on these test cases, we evaluate the mission performance and computational cost of the three models in TABLE X: the model in [16] which optimizes time and energy, the risk minimization model in Sec. III, and its deterministic version, where the capability uncertainties are not considered and the risk part, h_i , is removed from the objective function (17). Note that the model CTAS-O in [16] solves the same deterministic problem as the CTAS-D in this paper, but has a binary constraint for each agent (whether this agent is used or not). Therefore, CTAS-O does not use the flow decomposition described in Sec. V, but requires a binary variable for each individual agent instead of agent species. These additional binary constraints and variables expand the search space and reduce the scalability.

2) *Computational Cost and Discussion:* A 120-second time limitation is added to the solvers of the models. The optimality

Table IX: Task requirements. A value in the table is the requirement for that specific capability. γ is a scaling coefficient. E.g., the γ in (row 1, column 3) means task type m_1 requires the team's capability $a_3 \geq \gamma$. When γ is set larger, more agents get involved in the optimization and the problem space is larger. We do not scale non-cumulative capabilities. For one task, the requirements on different capability types are imposed with 'and' logic.

Task type	a_1	a_2	a_3	a_4	a_5	a_6	a_7	a_8	a_9
m_1 : Goods delivery								γ	
m_2 : Goods delivery (fly)	1							γ	
m_3 : Medical kits delivery			γ	γ					
m_4 : Contaminants removal								γ	γ
m_5 : Open area disinfection							γ	γ	2γ
m_6 : Quarantine enforcement			γ	γ	γ				γ
m_7 : Viral tests									γ
m_8 : Remote treatment								γ	γ

Table X: Three teaming models. 'Agent var' stands for 'agent variables'.

Model	Agent var	Objective	Variable number
CTAS-O [16]	Binary	Energy + Time	Large
CTAS-D	Real	Energy + Time	Relatively small
CTAS	Real	Energy + Time + Risk	Relatively small

gaps after the rounding process in Sec. V-B are given in Fig. 13a. Note that this gap is defined as (objective value - lower bound) / lower bound. The blue cells mean the solver cannot find a feasible solution for the specific case within the time limit. According to the two figures, CTAS-D and CTAS can solve much larger teaming problems. The largest problem that CTAS-D can deal with involves 140 agents and 40 tasks.

The increases of the optimality gaps due to the rounding process are shown in Fig. 13b. For most of the cases, the rounding process introduces an increase of the optimality gap within 1%. The leftmost cases have larger increases because the agent numbers are small, and rounding has larger overall influences. Since CTAS-O involves no rounding process, the increased gap is 0 for all test cases.

In these test cases, we assume the agent capabilities are Gaussian distributed. Therefore, given the estimation of the means and variances, we can calculate the probability of success. As shown in (50), the probability that a task can succeed equals the product of the probability that each capability requirement is satisfied. The mean probability is calculated according to (51).

$$P(\text{task } i \text{ succeeds}) = \prod_{\text{capability } a} P(a \text{ satisfied}) \quad \forall i \in M \quad (50)$$

$$\text{mean } P(\text{success}) = \left(\prod_{i \in M} P(\text{task } i \text{ succeeds}) \right)^{1/n_m} \quad (51)$$

The mean probabilities of success for the three models are shown in Fig. 14. For all cases, CTAS-O and CTAS-D models roughly result in a probability of 0.25. This is because each task requires two capabilities on average. When the risk is not considered, these two models tend only to match the expected requirement, and the probability of matching a single capability is 0.5. Clearly, the risk minimization model increases the probability of success for the tasks. In Fig. 15, we compare the result of CTAS to its deterministic version CTAS-D. With the chosen penalty coefficients on energy cost and task completion, i.e., C_e and C_h in equation (17), for most

of the test cases, a $\approx 20\%$ increase in energy cost introduce a $\approx 35\%$ increase in the mean probability of success. More importantly, the trade-off between energy cost and robustness depends on the penalty coefficients in the objective function and can be tuned smoothly. The trade-off gained by changing the penalty coefficients is shown in Fig. 17, using the smallest test case as an example.

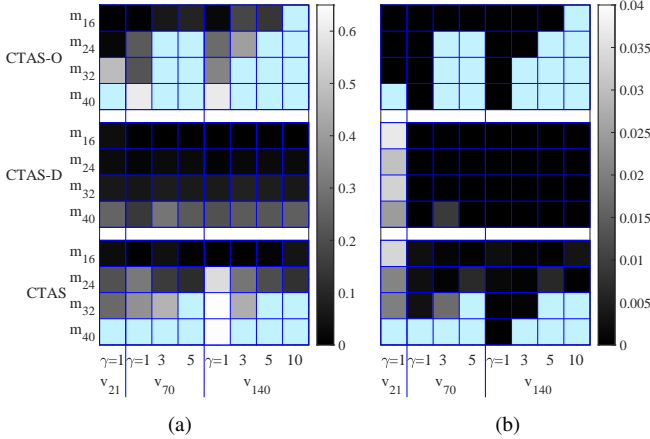


Fig. 13: The optimality gap of the three models applied to the 32 test cases. The colors correspond to the value specified in the color bars on the right. The blue cells mean the solver cannot find a feasible solution for the specific case within the time limit. (a) The optimality gap before the flow rounding process. The two white cells in the CTAS group are outliers whose values are around 1.0. (b) The increased optimality gap due to the rounding process.

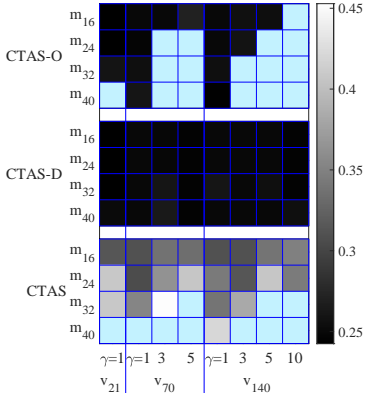


Fig. 14: The mean probability of success for the tasks using the three models.

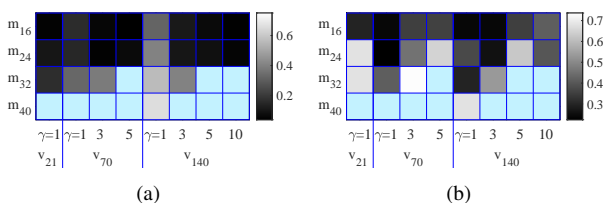


Fig. 15: Comparing the results of CTAS to CTAS-D. The values (colors) in the girds are (a) increased energy (relative) and (b) increased mean probability (relative) by adding the risk as an objective. I.e., the values are $(\text{CTAS} - \text{CTAS-D}) / \text{CTAS-D}$.

For the sample average approximation of the CVaR, we use 500 samples to approximate the assumed Gaussian distributions. Given the solution, we compare the nonlinear objectives

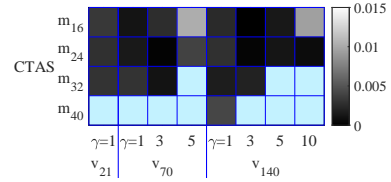


Fig. 16: The relative approximation gap of the nonlinear CVaR through sampling and linear programming.

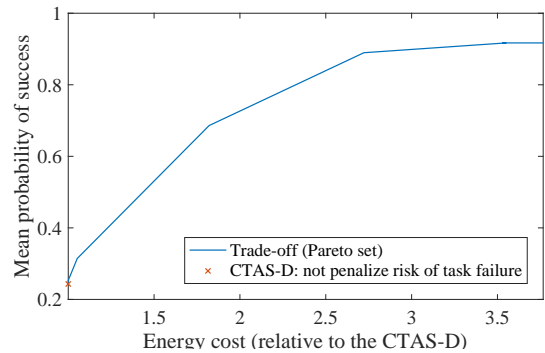


Fig. 17: Trade-off between energy cost and risk of task's non-completion for the case $\{16 \text{ tasks}, 21 \text{ agents}, \gamma = 1\}$.

to their sample approximations, and find that the relative approximation gaps are smaller than 1% for most of the cases as shown in Fig. 16. This shows that the approximation quality is good using 500 samples.

3) *Mission Performance and Discussion:* In this section, we take the test case with 16 tasks, 21 agents, and $\gamma = 1$ as an example to compare the solutions generated by the three models. In TABLE XI, we list the performance metrics and the probability of 5 tasks whose success rate is increased by the CTAS model. All three models are solved to optimal within the time limit. The models presented in this paper end up with much fewer variables for the same problem. By comparing CTAS with CTAS-D, we see that the risk minimization model reduces the CVaR and increases the probability of success for 5 tasks out of 16, with a small increase (5.3%) in the overall energy cost. Though CTAS-D and CTAS-O solve the same practical problem, the CTAS-D model, without explicit integer constraints on the number of agents, can fulfill the task requirements with lower cost before the rounding process and higher cost after.

The teams for the last 8 tasks are shown in TABLE XII. As expected, the CTAS model puts more agents in the team to reduce the CVaR. This task assignment is resulted from simultaneously considering the energy cost. As an example, CTAS puts more agents in the team of tasks m_9-m_{12} , but not tasks m_1-m_4 , even if they are of the same types. Because energy and time costs are jointly considered, and m_1-m_4 are far from the depot, adding more agents to ensure redundancy and robustness could potentially result in much higher costs. The risk minimization model also generates the routes and a consistent schedule. As an example, one v_1, v_4 , and v_5 visit task m_{13} at the same time as a team. The routes of species v_1, v_4 , and v_5 are shown in Fig. 18. These routes minimize overall travel distances and avoid the high-cost red regions to lower energy costs.

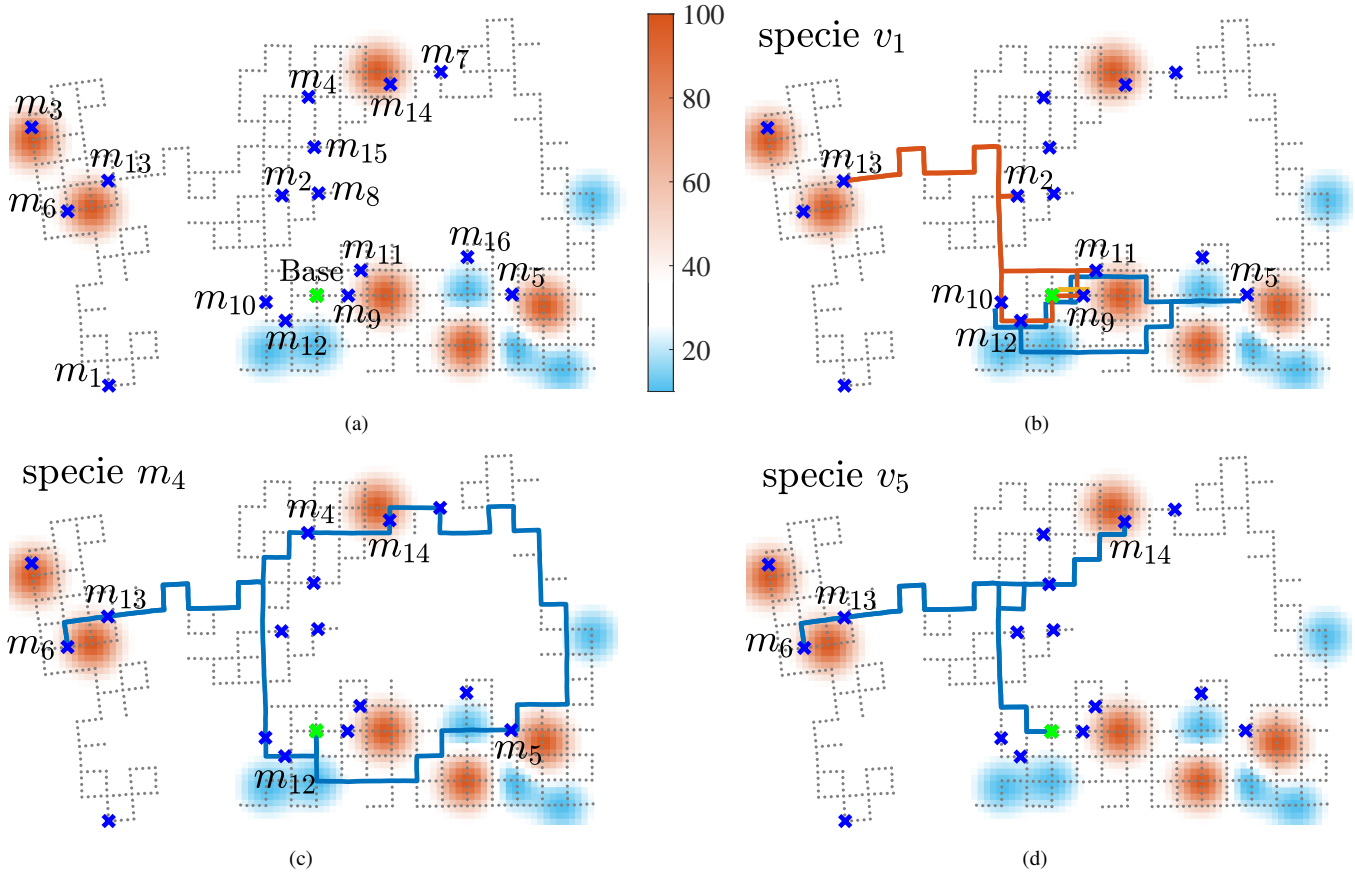


Fig. 18: (a) Task distribution: the 16 tasks are distributed in a city [58] where the unit travel cost depends on viral exposure. Blue and red stand for low and high energy costs, respectively. (b)-(d) The planned routes from the CTAS model for species v_1 , v_4 , and v_5 . Different colored lines represent distinct agent individuals from the same species.

Table XI: A comparison of the results of the three models. The $P(m_i)$, $i = 9, \dots, 13$ are the calculated probability of success for the specific tasks.

Item	CTAS-O	CTAS-D	CTAS
Variables	6194	4276	4384
Task CVaR	4.99×10^3	5.41×10^3	-1.03×10^4
Energy cost	2.06×10^5	2.06×10^5	2.17×10^5
$P(m_9)$	0.5	0.5	1
$P(m_{10})$	0.25	0.25	0.5
$P(m_{11})$	0.25	0.25	1
$P(m_{12})$	0.25	0.25	0.5
$P(m_{13})$	0.125	0.125	0.25

In summary, according to the teams in TABLE XII and routes in Fig. 18, the CTAS framework generates a consistent schedule for coordination, outputs routes that minimize energy costs, and assign tasks to agents such that redundancy is preserved at low costs to ensure a higher probability of task completion. The computational evaluation in Sec. VI-C2 shows that the frameworks CTAS and CTAS-D scale to 140 agents and 40 tasks with low optimality gaps. The scalability in agent number is better than the task number. Furthermore, CTAS-D still shows no optimality gap degeneration dealing with the largest test case we tested.

VII. CONCLUSIONS AND FUTURE WORK

This paper addresses a single-task robot multi-robot task time-extended assignment problem for complex tasks (CD-[ST-MR-TA]). We propose a mixed-integer programming

Table XII: Team configurations given by the three models. For task m_1 to m_8 , the three models output the same team configurations.

Task	CTAS-O	CTAS-D	CTAS
m_9	v_3	v_3	$v_1 \times 3, v_2 \times 3, v_3 \times 3$
m_{10}	v_1	v_1	$v_1 \times 2$
m_{11}	v_3	v_3	$v_1 \times 2, v_2 \times 3, v_3 \times 3$
m_{12}	v_4	v_4	$v_1 \times 2, v_4$
m_{13}	v_1, v_4	v_1, v_4	v_1, v_4, v_5
m_{14}	$v_2 \times 3, v_4, v_5$	$v_2 \times 3, v_4, v_5$	$v_2 \times 3, v_4, v_5$
m_{15}	v_7	v_7	v_7
m_{16}	v_7	v_7	v_7

model that simultaneously optimizes the task decomposition, assignment, and scheduling. The uncertainty within the team's capability is considered through risk minimization, and a robust metric, conditional value at risk (CVaR), is minimized to ensure robustness. The framework contributes to a domain-independent representation for complex tasks and heterogeneous agent capabilities that can generalize to multi-agent applications where the major goals are satisfying task-required capabilities. A two-step solution method is described, and the whole framework is evaluated in two different practical test cases. Results show that the framework is scalable to the number of agents and solves the problems with low optimality gaps. Given the selected hyper-parameters, the resulted assignments and schedules make a sensible trade-off between energy, time, and the probability of success. The task assignment

performance (apart from the scheduling) is also demonstrated through the comparison with the STRATA framework in the capture the flag case.

Future work will consider developing probabilistic learning methods that automatically estimate the parameters in the representation of task requirements and agent capabilities from current and previous task executions. Such learning methods would enable the possibility of closing the loop of the task assignment and scheduling, and iteratively improving the performance.

In future modeling choices, we will consider imposing a necessary and sufficient energy constraint in the CTAS model in Sec. III but still preserving the scalability of the current framework.

ACKNOWLEDGMENTS

DISTRIBUTION A. Approved for public release; distribution unlimited (OPSEC 5240). This research has been supported by the Automotive Research Center, a US Army center of excellence for modeling and simulation of ground vehicles.

REFERENCES

- [1] P. Tokekar, J. Vander Hook, D. Mulla, and V. Isler, “Sensor planning for a symbiotic uav and ugv system for precision agriculture,” *IEEE Trans. Robot.*, vol. 32, no. 6, pp. 1498–1511, 2016.
- [2] P. R. Wurman, R. D’Andrea, and M. Mountz, “Coordinating hundreds of cooperative, autonomous vehicles in warehouses,” *AI magazine*, vol. 29, no. 1, pp. 9–9, 2008.
- [3] J. Werfel, K. Petersen, and R. Nagpal, “Designing collective behavior in a termite-inspired robot construction team,” *Science*, vol. 343, no. 6172, pp. 754–758, 2014.
- [4] D. Shishika, J. Paulos, and V. Kumar, “Cooperative team strategies for multi-player perimeter-defense games,” *IEEE Robot. and Autom. Lett.*, vol. 5, no. 2, pp. 2738–2745, 2020.
- [5] X. Cai, B. Schlotfeldt, K. Khosoussi, N. Atanasov, G. J. Pappas, and J. P. How, “Non-monotone energy-aware information gathering for heterogeneous robot teams,” *arXiv preprint arXiv:2101.11093*, 2021.
- [6] M. Quann, L. Ojeda, W. Smith, D. Rizzo, M. Castanier, and K. Barton, “An energy-efficient method for multi-robot reconnaissance in an unknown environment,” in *Proc. Amer. Control Conf.* IEEE, 2017, pp. 2279–2284.
- [7] ——, “Ground robot terrain mapping and energy prediction in environments with 3-d topography,” in *Proc. Amer. Control Conf.* IEEE, 2018, pp. 3532–3537.
- [8] ——, “Chance constrained reachability in environments with spatially varying energy costs,” *Robot. and Auton. Syst.*, vol. 119, pp. 1–12, 2019.
- [9] ——, “Power prediction for heterogeneous ground robots through spatial mapping and sharing of terrain data,” *IEEE Robot. and Autom. Lett.*, vol. 5, no. 2, pp. 1579–1586, 2020.
- [10] B. Schlotfeldt, V. Tzoumas, D. Thakur, and G. J. Pappas, “Resilient active information gathering with mobile robots,” in *Proc. IEEE/RSJ Int. Conf. Intell. Robots and Syst.* IEEE, 2018, pp. 4309–4316.
- [11] K. Yu, J. M. O’Kane, and P. Tokekar, “Coverage of an environment using energy-constrained unmanned aerial vehicles,” in *Proc. IEEE Int. Conf. Robot. and Automation.* IEEE, 2019, pp. 3259–3265.
- [12] Y. Sung, A. K. Budhiraja, R. K. Williams, and P. Tokekar, “Distributed assignment with limited communication for multi-robot multi-target tracking,” *Auton. Robot.*, vol. 44, no. 1, pp. 57–73, 2020.
- [13] Y. Tan and Z.-y. Zheng, “Research advance in swarm robotics,” *Defence Technology*, vol. 9, no. 1, pp. 18–39, 2013.
- [14] K. Sundar, S. Venkatachalam, and S. G. Manyam, “Path planning for multiple heterogeneous unmanned vehicles with uncertain service times,” in *Proc. of the Int. Conf. on Unmanned Aircraft Syst.*, 2017, pp. 480–487.
- [15] G. A. Korsah, A. Stentz, and M. B. Dias, “A comprehensive taxonomy for multi-robot task allocation,” *Int. J. Robot. Res.*, vol. 32, no. 12, pp. 1495–1512, 2013.
- [16] B. Fu, W. Smith, D. Rizzo, M. Castanier, and K. Barton, “Heterogeneous vehicle routing and teaming with gaussian distributed energy uncertainty,” in *Proc. IEEE/RSJ Int. Conf. Intell. Robots and Syst.* IEEE, 2020, pp. 4315–4322.
- [17] B. P. Gerkey and M. J. Matarić, “A formal analysis and taxonomy of task allocation in multi-robot systems,” *Int. J. Robot. Res.*, vol. 23, no. 9, pp. 939–954, 2004.
- [18] S. D. Ramchurn, M. Polukarov, A. Farinelli, N. Jennings, and C. Trong, “Coalition formation with spatial and temporal constraints,” *Proc. of the Int. Conf. on Auton. Agents and Multiagent Syst.*, 2010.
- [19] G. A. Korsah, B. Kannan, B. Browning, A. Stentz, and M. B. Dias, “xbots: An approach to generating and executing optimal multi-robot plans with cross-schedule dependencies,” in *Proc. IEEE Int. Conf. Robot. and Automation.* IEEE, 2012, pp. 115–122.
- [20] C. Özgüven, Y. Yavuz, and L. Özbaşır, “Mixed integer goal programming models for the flexible job-shop scheduling problems with separable and non-separable sequence dependent setup times,” *Applied Mathematical Modelling*, vol. 36, no. 2, pp. 846–858, 2012.
- [21] W.-Y. Ku and J. C. Beck, “Mixed integer programming models for job shop scheduling: A computational analysis,” *Computers & Operations Research*, vol. 73, pp. 165–173, 2016.
- [22] J. Moser, J. Hoffman, R. Hildebrand, and E. Komendera, “A flexible job shop scheduling representation of the autonomous in-space assembly task assignment problem,” *arXiv preprint arXiv:2003.12148*, 2020.
- [23] S. Liemhetcharat and M. Veloso, “Modeling mutual capabilities in heterogeneous teams for role assignment,” in *Proc. IEEE/RSJ Int. Conf. Intell. Robots and Syst.* IEEE, 2011, pp. 3638–3644.
- [24] ——, “Weighted synergy graphs for role assignment in ad hoc heterogeneous robot teams,” in *Proc. IEEE/RSJ Int. Conf. Intell. Robots and Syst.* IEEE, 2012, pp. 5247–5254.
- [25] E. G. Jones, M. B. Dias, and A. Stentz, “Time-extended multi-robot coordination for domains with intra-path constraints,” *Auton. Robot.*, vol. 30, no. 1, pp. 41–56, 2011.
- [26] M. Pujol-Gonzalez, J. Cerquides, P. Meseguer, and J. A. Rodríguez-Aguilar, “Efficient inter-team task allocation in robocup rescue,” *Proc. of the Int. Conf. on Auton. Agents and Multiagent Syst.*, 2015.
- [27] S. D. Klee, G. Gemignani, D. Nardi, and M. Veloso, “Graph-based task libraries for robots: Generalization and autocompletion,” in *Congress of the Italian Association for Artificial Intelligence.* Springer, 2015, pp. 397–409.
- [28] M. N. Nicolescu and M. J. Mataric, “Natural methods for robot task learning: Instructive demonstrations, generalization and practice,” in *Proceedings of the second international joint conference on Autonomous agents and multiagent systems*, 2003, pp. 241–248.
- [29] S. Ekvall and D. Kragic, “Robot learning from demonstration: a task-level planning approach,” *International Journal of Advanced Robotic Systems*, vol. 5, no. 3, p. 33, 2008.
- [30] S. Nieku, S. Osentoski, G. Konidaris, and A. G. Barto, “Learning and generalization of complex tasks from unstructured demonstrations,” in *Proc. IEEE/RSJ Int. Conf. Intell. Robots and Syst.* IEEE, 2012, pp. 5239–5246.
- [31] D. H. Grollman and O. C. Jenkins, “Incremental learning of subtasks from unsegmented demonstration,” in *Proc. IEEE/RSJ Int. Conf. Intell. Robots and Syst.* IEEE, 2010, pp. 261–266.
- [32] B. Hayes and B. Scassellati, “Effective robot teammate behaviors for supporting sequential manipulation tasks,” in *Proc. IEEE/RSJ Int. Conf. Intell. Robots and Syst.* IEEE, 2015, pp. 6374–6380.
- [33] C. Galindo, J.-A. Fernández-Madrigal, J. González, and A. Saffiotti, “Robot task planning using semantic maps,” *Robot. and Auton. Syst.*, vol. 56, no. 11, pp. 955–966, 2008.
- [34] C. Aeronautiques, A. Howe, C. Knoblock, I. D. McDermott, A. Ram, M. Veloso, D. Weld, D. W. SRI, A. Barrett, D. Christianson, *et al.*, “Pddl—the planning domain definition language,” 1998.
- [35] A. Torreño, E. Onaindia, A. Komenda, and M. Štolba, “Cooperative multi-agent planning: A survey,” *ACM Computing Surveys (CSUR)*, vol. 50, no. 6, pp. 1–32, 2017.
- [36] D. Song, K. Huebner, V. Kyriki, and D. Kragic, “Learning task constraints for robot grasping using graphical models,” in *Proc. IEEE/RSJ Int. Conf. Intell. Robots and Syst.* IEEE, 2010, pp. 1579–1585.
- [37] C. H. Ek, D. Song, K. Huebner, and D. Kragic, “Task modeling in imitation learning using latent variable models,” in *Proc. of the IEEE-RAS Int. Conf. Humanoid Robots.* IEEE, 2010, pp. 548–553.
- [38] R. Zlot and A. Stentz, “Multirobot control using task abstraction in a market framework,” in *Collaborative Technology Alliances Conference*, 2003.
- [39] ——, “Market-based multirobot coordination using task abstraction,” in *Field and Service Robotics.* Springer, 2003, pp. 167–177.

[40] ——, “Complex task allocation for multiple robots,” in *Proc. IEEE Int. Conf. Robot. and Automation*. IEEE, 2005, pp. 1515–1522.

[41] B. Hayes and B. Scassellati, “Autonomously constructing hierarchical task networks for planning and human-robot collaboration,” in *Proc. IEEE Int. Conf. Robot. and Automation*. IEEE, 2016, pp. 5469–5476.

[42] F. Faruq, D. Parker, B. Lacorda, and N. Hawes, “Simultaneous task allocation and planning under uncertainty,” in *Proc. IEEE/RSJ Int. Conf. Intell. Robots and Syst.* IEEE, 2018, pp. 3559–3564.

[43] H. Ravichandar, K. Shaw, and S. Chernova, “Strata: unified framework for task assignments in large teams of heterogeneous agents,” *Autonomous Agents and Multi-Agent Systems*, vol. 34, no. 2, 2020.

[44] A. Majumdar and M. Pavone, “How should a robot assess risk? towards an axiomatic theory of risk in robotics,” in *Robotics Research*. Springer, 2020, pp. 75–84.

[45] L. Zhou and P. Tokekar, “An approximation algorithm for risk-averse submodular optimization,” in *International Workshop on the Algorithmic Foundations of Robotics*. Springer, 2018, pp. 144–159.

[46] R. Balasubramanian, L. Zhou, P. Tokekar, and P. Sujit, “Risk-aware submodular optimization for multi-objective travelling salesperson problem,” *arXiv preprint arXiv:2011.01095*, 2020.

[47] J. Bernhard, S. Pollok, and A. Knoll, “Addressing inherent uncertainty: Risk-sensitive behavior generation for automated driving using distributional reinforcement learning,” in *Proc. IEEE Intell. Veh. Symp.* IEEE, 2019, pp. 2148–2155.

[48] L. Lindemann, G. J. Pappas, and D. V. Dimarogonas, “Control barrier functions for nonholonomic systems under risk signal temporal logic specifications,” in *Proc. IEEE Conf. Decision Control*. IEEE, 2020, pp. 1422–1428.

[49] A. Hakobyan, G. C. Kim, and I. Yang, “Risk-aware motion planning and control using cvar-constrained optimization,” *IEEE Robot. and Autom. Lett.*, vol. 4, no. 4, pp. 3924–3931, 2019.

[50] A. Prorok, M. A. Hsieh, and V. Kumar, “The impact of diversity on optimal control policies for heterogeneous robot swarms,” *IEEE Trans. Robot.*, vol. 33, no. 2, pp. 346–358, 2017.

[51] R. T. Rockafellar, S. Uryasev, *et al.*, “Optimization of conditional value-at-risk,” *Journal of risk*, vol. 2, pp. 21–42, 2000.

[52] S. Asmussen and P. W. Glynn, *Stochastic simulation: algorithms and analysis*. Springer Science & Business Media, 2007, vol. 57.

[53] J. R. Birge and F. Louveaux, *Introduction to stochastic programming*. Springer Science & Business Media, 2011.

[54] I. Heller and C. Tompkins, “An extension of a theorem of dantzig’s,” *Linear inequalities and related systems*, vol. 38, pp. 247–254, 1956.

[55] T. Barfoot, J. Burgner-Kahrs, E. Diller, A. Garg, A. Goldenberg, J. Kelly, X. Liu, H. Naguib, G. Nejat, A. Schoellig, *et al.*, “Making sense of the robotized pandemic response: a comparison of global and canadian robot deployments and success factors,” *arXiv preprint arXiv:2009.08577*, 2020.

[56] A. A. Malik, T. Masood, and R. Kousar, “Repurposing factories with robotics in the face of covid-19,” *Science Robotics*, vol. 5, no. 43, 2020.

[57] V. Chamola, V. Hassija, V. Gupta, and M. Guizani, “A comprehensive review of the covid-19 pandemic and the role of iot, drones, ai, blockchain, and 5g in managing its impact,” *IEEE Access*, vol. 8, pp. 90 225–90 265, 2020.

[58] E. Olson, J. Leonard, and S. Teller, “Fast iterative alignment of pose graphs with poor initial estimates,” in *Proc. IEEE Int. Conf. Robot. and Automation*. IEEE, 2006, pp. 2262–2269.

[59] C. K. Williams and C. E. Rasmussen, *Gaussian processes for machine learning*. MIT press Cambridge, MA, 2006, vol. 2, no. 3.